Computers and Structures 225 (2019)

Contents lists available at ScienceDirect

Computers and Structures

journal homepage: www.elsevier.com/locate/compstruc

For direct time integrations: A comparison of the Newmark and ρ_∞-Bathe schemes

Gunwoo Noh [a,*], Klaus-Jürgen Bathe [b]

[a] Kyungpook National University, Daegu 41566, Republic of Korea
[b] Massachusetts Institute of Technology, Cambridge, MA 02139, USA

ARTICLE INFO

Article history:
Received 1 April 2019
Accepted 26 May 2019

Keywords:
Transient analyses
Direct time integrations
Implicit and explicit schemes
Stability and accuracy
Newmark and Bathe methods
Dissipation and dispersion

ABSTRACT

We consider the unconditionally stable Newmark and ρ_∞-Bathe methods for the direct time integration of the finite element equations in structural dynamics and wave propagations. In our evaluation of the Newmark method we consider the parameters δ and α, and in the ρ_∞-Bathe method we consider the parameters γ and ρ_∞, with $0 < \gamma < \infty$, $\gamma \neq 1$ and $\rho_\infty \in [-1, +1]$. We show that the Newmark method as usually used with its δ and α parameters, $\alpha = 0.25(\delta + 0.5)^2$ and $\delta \geqslant 0.5$, is a special case of the ρ_∞-Bathe method. We also show that the β_1/β_2-Bathe method is a special case of the ρ_∞-Bathe scheme. The study of the curves of numerical dissipation and dispersion shows that the ρ_∞-Bathe method provides effective dissipation and dispersion whereas the Newmark method lacks in that regard. To illustrate our theoretical findings we give the results of some example solutions of structural dynamics and wave propagations. Our study also shows that further research is needed to identify the optimal use of the ρ_∞-Bathe scheme and other implicit methods in wave propagation analyses.

1. Introduction

The direct time integration of the finite element equations governing structural response and wave propagations is now widely performed in industry and the sciences. In linear analysis, other approaches can be used, like the method of mode superposition, but in nonlinear analysis, the direct time integration is commonly pursued [1–3].

For the integration, explicit and implicit schemes are used. The explicit schemes are generally conditionally stable and are used with very small time steps for short duration events, like crush simulations and short time wave propagations. The implicit schemes employed are generally unconditionally stable, are used with larger time steps in structural dynamics and also in the simulation of wave propagations. The premise of an implicit method is that it can be used with larger time steps, thus requiring much less time steps in a simulation. Hence, although the computational time per time step is much larger than for an explicit scheme, the total solution cost is less than for an explicit scheme. In addition, an implicit solution of a problem is frequently also more robust than an explicit solution [3].

A large number of explicit and implicit time integration schemes has been proposed and analyzed [4–22]. However, the search for more effective methods has continued because the available schemes showed short-comings and any increase in effectiveness can be of much value in engineering and scientific analyses.

Until about a decade ago, this search focused on requiring that only the equilibrium at the time points t and $t + \Delta t$ be considered in the time integration, where Δt denotes the time step. However, there is of course no reason to not consider also time points other than t and $t + \Delta t$, such as the use of a composite scheme, provided that scheme using more equilibrium points is in the overall solution more effective.

The first implicit composite schemes for structural dynamics were probably proposed in Refs. [23,24]. The Bathe method of time integration using two sub-steps per time step has found considerable use, was analysed in refs. [25–27], and extensions were proposed [28,29]. Other composite time integration schemes including explicit schemes were also proposed, see Refs. [30–39].

A very widely used implicit time integration scheme is the unconditionally stable Newmark method with its two parameters α and δ and in particular the trapezoidal rule with $\alpha = 0.25$ and $\delta = 0.5$.

Our objective in this paper is to study the Newmark method and the ρ_∞-Bathe scheme, compare the schemes and elucidate differences in solution accuracy when considering typical finite element

* Corresponding author.
E-mail address: gunwoo@knu.ac.kr (G. Noh).

https://doi.org/10.1016/j.compstruc.2019.05.015
0045-7949/

analyses. Since the Bathe method uses two sub-steps per time step Δt, we also use two sub-steps in the Newmark method; in this way the solution effort per step is about the same. Our findings are that the Newmark method, as typically used in practice, is a special case of the ρ_∞-Bathe method and that the Bathe scheme, when used in its optimal setting, shows much better dissipation and dispersion characteristics.

2. The ρ_∞-Bathe method and the two-step Newmark method

In this section we briefly review the time integration schemes that we will compare and evaluate in the paper.

2.1. Basic equations and properties

In the ρ_∞-Bathe method [29], we calculate the unknown displacements, velocities, and accelerations by considering the time step Δt to consist of two sub-steps. The sub-step sizes are $\gamma\Delta t$ and $(1-\gamma)\Delta t$ for the first and second sub-steps, respectively.

In the first sub-step, we use the trapezoidal rule for the equilibrium at time $t+\gamma\Delta t$,

$$\mathbf{M}^{t+\gamma\Delta t}\ddot{\mathbf{U}} + \mathbf{C}^{t+\gamma\Delta t}\dot{\mathbf{U}} + \mathbf{K}^{t+\gamma\Delta t}\mathbf{U} = {}^{t+\gamma\Delta t}\mathbf{R} \tag{1}$$

$${}^{t+\gamma\Delta t}\mathbf{U} = {}^{t}\mathbf{U} + \frac{\gamma\Delta t}{2}({}^{t}\dot{\mathbf{U}} + {}^{t+\gamma\Delta t}\dot{\mathbf{U}}) \tag{2}$$

$${}^{t+\gamma\Delta t}\dot{\mathbf{U}} = {}^{t}\dot{\mathbf{U}} + \frac{\gamma\Delta t}{2}({}^{t}\ddot{\mathbf{U}} + {}^{t+\gamma\Delta t}\ddot{\mathbf{U}}) \tag{3}$$

and in the second sub-step, we use the following relations for the equilibrium at time $t+\Delta t$.

$$\mathbf{M}^{t+\Delta t}\ddot{\mathbf{U}} + \mathbf{C}^{t+\Delta t}\dot{\mathbf{U}} + \mathbf{K}^{t+\Delta t}\mathbf{U} = {}^{t+\Delta t}\mathbf{R} \tag{4}$$

$${}^{t+\Delta t}\mathbf{U} = {}^{t}\mathbf{U} + \Delta t(q_0{}^{t}\dot{\mathbf{U}} + q_1{}^{t+\gamma\Delta t}\dot{\mathbf{U}} + q_2{}^{t+\Delta t}\dot{\mathbf{U}}) \tag{5}$$

$${}^{t+\Delta t}\dot{\mathbf{U}} = {}^{t}\dot{\mathbf{U}} + \Delta t(s_0{}^{t}\ddot{\mathbf{U}} + s_1{}^{t+\gamma\Delta t}\ddot{\mathbf{U}} + s_2{}^{t+\Delta t}\ddot{\mathbf{U}}) \tag{6}$$

where $\mathbf{M}$, $\mathbf{C}$, $\mathbf{K}$ are the mass, damping and stiffness matrices, and the vectors $\mathbf{U}$ and $\mathbf{R}$ list, respectively, the nodal displacements (rotations) and externally applied nodal forces (moments). An overdot denotes a time derivative.

The parameters in Eqs. (5) and (6), $s_0, s_1, s_2, q_0, q_1, q_2, \gamma$, can be determined in various ways. In our previous work, we considered the conditions for unconditional stability in linear analysis, second-order accuracy, and complex conjugate eigenvalues of the approximation matrix for all Ω_0 where $\Omega_0 = \omega_0\Delta t$ with ω_0 the modal natural frequency.

To have second-order accuracy, we use

$$\begin{aligned} q_0 &= (\gamma-1)q_1 + \tfrac{1}{2} \\ q_2 &= -\gamma q_1 + \tfrac{1}{2} \\ s_0 &= (\gamma-1)s_1 + \tfrac{1}{2} \\ s_2 &= -\gamma s_1 + \tfrac{1}{2} \end{aligned} \tag{7}$$

and to have unconditional stability with the complex conjugate eigenvalues for all Ω_0 we use

$$s_1 = q_1 \tag{8}$$

Lastly, to directly prescribe the amount of numerical dissipation in the high frequency range, we use the relation between q_1, γ and a new parameter, ρ_∞:

$$q_1 = \frac{\rho_\infty + 1}{2\gamma(\rho_\infty - 1) + 4} \tag{9}$$

where

$$\lim_{\Omega_0\to\infty} \rho(\mathbf{A}_{\rho_\infty\text{-Bathe}}) = |\rho_\infty|, \quad \rho_\infty \in [-1,1] \tag{10}$$

The scheme has then two free parameters, γ and ρ_∞. Previously we only considered $\rho_\infty \in [0,1]$ but the negative values of $\rho_\infty \in [-1,0]$ may also be used, and some benefits using a negative value can arise, see Sections 2.3 and 3.2.

Using $\rho_\infty \in [0,1]$, the scheme provides the same effective stiffness matrix for each sub-step, a local maximum of amplitude decay and the global minimum of period elongation with the following value for γ:

$$\gamma_0 = \frac{2-\sqrt{2+2\rho_\infty}}{1-\rho_\infty}; \quad \gamma_0 = 0.5 \quad \text{if } \rho_\infty = 1 \tag{11}$$

With the relation in Eq. (11), the method is a one-parameter scheme and it is in that sense optimal for $\rho_\infty \in [0,1]$, $\gamma \in (0,\ 1)$.

Fig. 1 shows the spectral radii, percentage period elongations and numerical damping ratios of the ρ_∞-Bathe method with $\gamma = 0.5$ and γ_0 for various values of ρ_∞. The values $\gamma = 0.5$ and $\gamma = \gamma_0$ provide practically the same curves for all $\rho_\infty \in [0,1]$.

Next, we consider the usual use of the Newmark method [3,5]. To compare the Newmark and ρ_∞-Bathe methods using the same computational costs, we employ the two-step Newmark method with the sub-step sizes $(\Delta t/2)$.

In the first sub-step of the two-step Newmark method, we consider the equilibrium at time $t+\Delta t/2$

$$\mathbf{M}^{t+\Delta t/2}\ddot{\mathbf{U}} + \mathbf{C}^{t+\Delta t/2}\dot{\mathbf{U}} + \mathbf{K}^{t+\Delta t/2}\mathbf{U} = {}^{t+\Delta t/2}\mathbf{R} \tag{12}$$

$${}^{t+\Delta t/2}\dot{\mathbf{U}} = {}^{t}\dot{\mathbf{U}} + [(1-\delta){}^{t}\ddot{\mathbf{U}} + \delta^{t+\Delta t/2}\ddot{\mathbf{U}}](\Delta t/2) \tag{13}$$

$${}^{t+\Delta t/2}\mathbf{U} = {}^{t}\mathbf{U} + {}^{t}\dot{\mathbf{U}}(\Delta t/2) + [(1/2-\alpha){}^{t}\ddot{\mathbf{U}} + \alpha^{t+\Delta t/2}\ddot{\mathbf{U}}](\Delta t/2)^2 \tag{14}$$

and in the second sub-step we consider the equilibrium at time $t+\Delta t$

$$\mathbf{M}^{t+\Delta t}\ddot{\mathbf{U}} + \mathbf{C}^{t+\Delta t}\dot{\mathbf{U}} + \mathbf{K}^{t+\Delta t}\mathbf{U} = {}^{t+\Delta t}\mathbf{R} \tag{15}$$

$${}^{t+\Delta t}\dot{\mathbf{U}} = {}^{t+\Delta t/2}\dot{\mathbf{U}} + [(1-\delta)^{t+\Delta t/2}\ddot{\mathbf{U}} + \delta^{t+\Delta t}\ddot{\mathbf{U}}](\Delta t/2) \tag{16}$$

$$\begin{aligned} {}^{t+\Delta t}\mathbf{U} = {}^{t+\Delta t/2}\mathbf{U} + {}^{t+\Delta t/2}\dot{\mathbf{U}}(\Delta t/2) + [(1/2-\alpha)^{t+\Delta t/2}\ddot{\mathbf{U}} \\ + \alpha^{t+\Delta t}\ddot{\mathbf{U}}](\Delta t/2)^2 \end{aligned} \tag{17}$$

The method is unconditionally stable when $\delta \geqslant 0.5$ and $\alpha \geqslant 0.25(\delta+0.5)^2$. The method is a non-dissipative second-order accurate method when $\delta = 0.5$, and a dissipative first-order accurate method otherwise. The method is the commonly called trapezoidal rule when $\delta = 0.5$ and $\alpha = 0.25$.

From now on we frequently refer to the Newmark method using two equal sub-steps per time step simply as the Newmark method. Although then not explicitly stated, we always use these two sub-steps.

Considering a given value of δ, the value $\alpha = 0.25(\delta+0.5)^2$ provides the least period elongation and a larger value of δ results into more numerical damping. For the case of $\alpha = 0.25(\delta+0.5)^2$, the ultimate spectral radius of the Newmark method is

$$\lim_{\Omega_0\to\infty} \rho(\mathbf{A}_{\text{Newmark}}) = \frac{(2\delta-3)^2}{(2\delta+1)^2}\ , \ \delta \geqslant 0.5 \tag{18}$$

As δ increases from 0.5 to 1.5, the ultimate spectral radius decreases from 1 to 0, and as δ increases from 1.5 to ∞, the ultimate spectral radius increases from 0 to 1.

Figs. 2 and 3 show the spectral radii, period elongations, and numerical damping ratios of the Newmark method for various values of κ and δ where $\alpha = \kappa\ (\delta+0.5)^2$. We can make a number of observations:

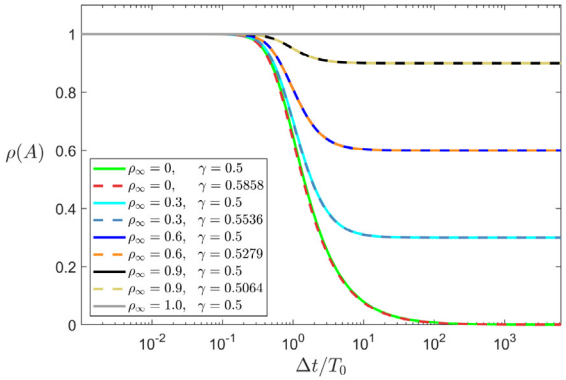

(a) Spectral radii of approximation operator of the ρ_∞- Bathe method

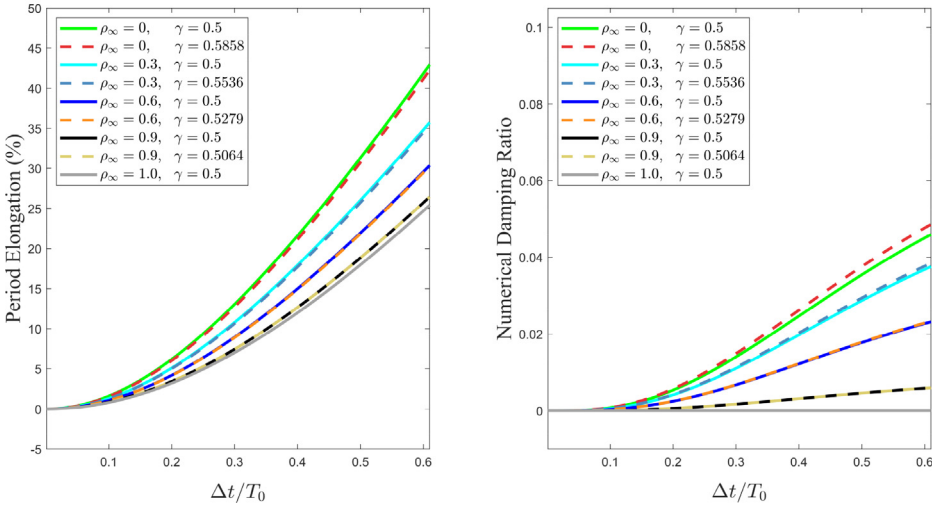

(b) Percentage period elongation and numerical damping ratio of the ρ_∞- Bathe method

Fig. 1. The ρ_∞-Bathe method when $\xi = 0$ with $\gamma = 0.5$ (solid line) and $\gamma = \gamma_0$ given in Eq. (11) (dashed line) for various values of $\rho_\infty \in [0, 1]$.

- Firstly, for a given value of δ, using $\alpha = 0.25(\delta + 0.5)^2$ in the Newmark method provides maximum numerical dissipation and minimum numerical dispersion.
- Secondly, the numerical dissipation curves have only an "acceptable shape" for the case $\alpha = 0.25\ (\delta + 0.5)^2$ and $0.5 \leqslant \delta \leqslant 1.5$ but even in that case the curves have the opposite curvatures to those of the ρ_∞-Bathe scheme, see Fig. 1. The best curvature gives very little damping at small time steps and rapidly increasing damping at larger time steps, with the numerical damping ratio continuously increasing as $\Delta t/T_0$ increases (as shown in Fig. 1).

Since it is important to have strong numerical dissipation for the higher modes in the direct time integration, using δ to control the dissipation, the Newmark method provides its best performance with $\alpha = 0.25(\delta + 0.5)^2$ and $0.5 \leqslant \delta \leqslant 1.5$.

2.2. Relations between the ρ_∞-Bathe method and the Newmark method

We can directly show that the ρ_∞-Bathe method with $\rho_\infty = 1$ and $\gamma = 1/2$, corresponds to the Newmark method using $\alpha = 1/4$ and $\delta = 1/2$, see Appendix A. However, when $\gamma \neq 1/2$ a direct comparison is not straightforward. Therefore we compare the characteristic polynomials of the integration approximation matrices of the Newmark and ρ_∞-Bathe methods: identical characteristic polynomials provide identical spectral properties.

In the modal equations, the ρ_∞-Bathe method and the Newmark method may be expressed in the form

$$\begin{bmatrix} {}^{t+\Delta t}\ddot{x} \\ {}^{t+\Delta t}\dot{x} \\ {}^{t+\Delta t}x \end{bmatrix} = \mathbf{A} \begin{bmatrix} {}^{t}\ddot{x} \\ {}^{t}\dot{x} \\ {}^{t}x \end{bmatrix} + \mathbf{L_a}\,{}^{t+\gamma\Delta t}r + \mathbf{L_b}\,{}^{t+\Delta t}r \tag{19}$$

where $\mathbf{A}$, $\mathbf{L_a}$ and $\mathbf{L_b}$ are the integration approximation and load operators, respectively, and x denotes the displacement in modal space. The characteristic polynomials of $\mathbf{A}$ of both methods have the form:

$$p(\lambda) = \lambda^3 - 2A_1\lambda^2 + A_2\lambda - A_3 \tag{20}$$

Considering the physical case of no damping, the coefficients of the characteristic polynomial of the ρ_∞-Bathe method are

$$\begin{aligned} A_1|_{\rho_\infty-\text{Bathe}} &= -\frac{1}{2\beta_{01}\beta_{02}}(\gamma^2((s_0-s_1)q_2+s_2(q_0-q_1))\Omega_0^4 \\ &\quad +(-2\gamma^2+4\gamma(q_1+s_1)+4q_2(s_0+s_1)+4s_2(q_0+q_1))\Omega_0^2-8); \\ A_2|_{\rho_\infty-\text{Bathe}} &= \frac{1}{\beta_{01}\beta_{02}}(\gamma^2(s_0-s_1)(q_0-q_1)\Omega_0^4 \\ &\quad +(\gamma^2-4(q_1+s_1)\gamma+4(s_0+s_1)(q_0+q_1))\Omega_0^2+4)); \end{aligned} \tag{21}$$

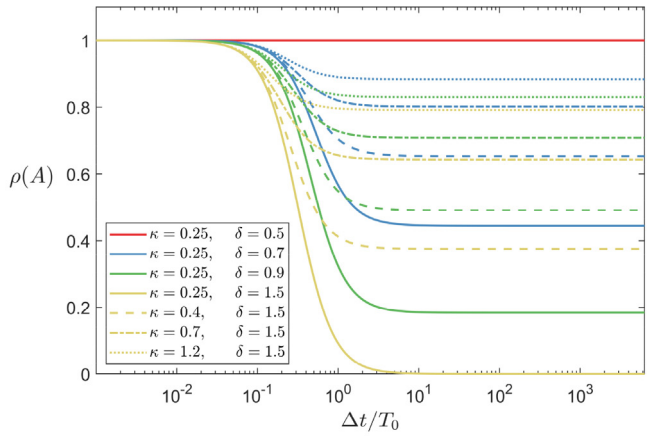

(a) Spectral radii of approximation operator of the two-step Newmark method for $\delta \leq 1.5$

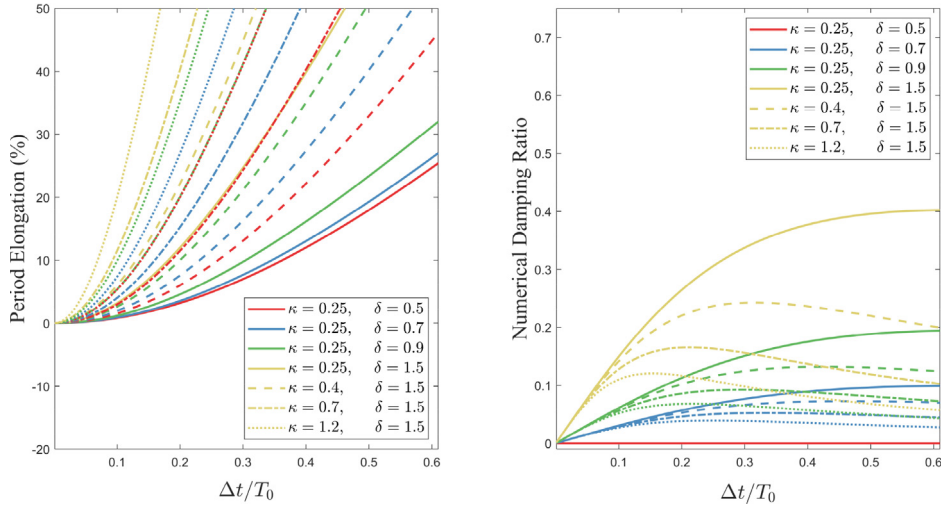

(b) Percentage period elongation and numerical damping ratio of the two-step Newmark method for $\delta \leq 1.5$

Fig. 2. The two-step Newmark method when $\xi = 0$ with $\alpha = \kappa(\delta + 0.5)^2$ for various values of κ and $\delta \leqslant 1.5$; Each color indicates a value of δ; Each line type indicates a value of κ: solid ($\kappa = 0.25$), dashed ($\kappa = 0.4$), dashed dot ($\kappa = 0.7$), dotted ($\kappa = 1.2$).

$$A_3|_{\rho_\infty-\text{Bathe}} = 0 \ ;$$

$$\beta_{01} = \Omega_0^2\gamma^2 + 4; \ \beta_{02} = 1 + q_2 s_2 \Omega_0^2$$

and of the Newmark method are

$$A_1|_{\text{Newmark}} = \tfrac{1}{8\zeta}(128 + (64\alpha - 32\delta - 48)\Omega_0^2 + (8\alpha^2 + (-8\delta - 12)\alpha + 4(\delta + 1/2)^2)\Omega_0^4 \ ) \ ;$$

$$A_2|_{\text{Newmark}} = \frac{1}{\zeta}\left(4 + \left(\alpha - \delta + \frac{1}{2}\right)\Omega_0^2\right)^2 ; \tag{22}$$

$$A_3|_{\text{Newmark}} = 0;$$

$$\zeta = (\Omega_0^2\alpha + 4)^2;$$

Using Eqs. (21) and (22), the relations to have identical characteristic polynomials of the amplification matrices are:

$$\alpha = \frac{1}{2}\gamma^2 + 2q_2 s_2$$

$$\alpha^2 = 4q_2 s_2 \gamma^2$$

$$\alpha - \frac{\delta}{2} - \frac{3}{4} = \frac{1}{2}\gamma^2 - (q_1 + s_1)\gamma - q_1 s_2 - (s_0 + s_1)q_2 - q_0 s_2$$

$$\alpha - \delta + \frac{1}{2} = \frac{1}{2}\gamma^2 - 2(q_1 + s_1)\gamma + 2(s_0 + s_1)(q_0 + q_1) \tag{23}$$

$$\alpha^2 - \left(\delta + \frac{3}{2}\right)\alpha + \frac{1}{2}\left(\delta + \frac{1}{2}\right)^2 = -2((s_0 - s_1)q_2 + s_2(q_0 - q_1))\gamma^2$$

$$\left(\alpha - \delta + \frac{1}{2}\right)^2 = 4\gamma^2(s_0 - s_1)(q_0 - q_1)$$

Due to the nonlinear nature of the relations in Eq. (23), it is not feasible to obtain explicit expressions of $s_0, s_1, s_2, q_0, q_1, q_2$ and γ in terms of the parameters of the Newmark method for arbitrary α and δ. However, with the relations in Eqs. (7)–(9), we find that the unique solution of Eq. (23) is

$$\alpha = 1/4, \quad \delta = 1/2, \quad \rho_\infty = 1, \quad \gamma = 1/2 \tag{24}$$

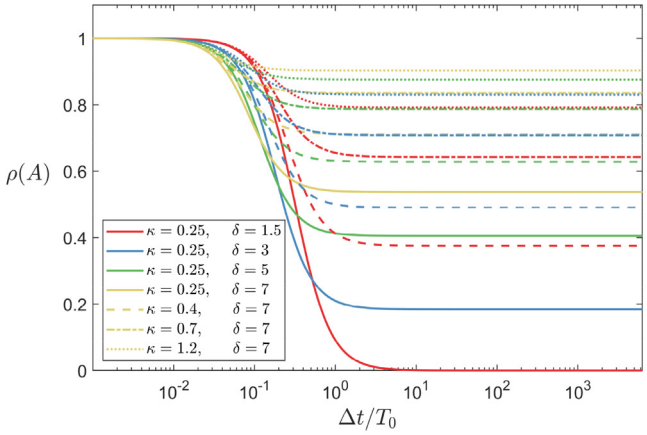

(a) Spectral radii of approximation operator of the two-step Newmark method for $\delta \geq 1.5$

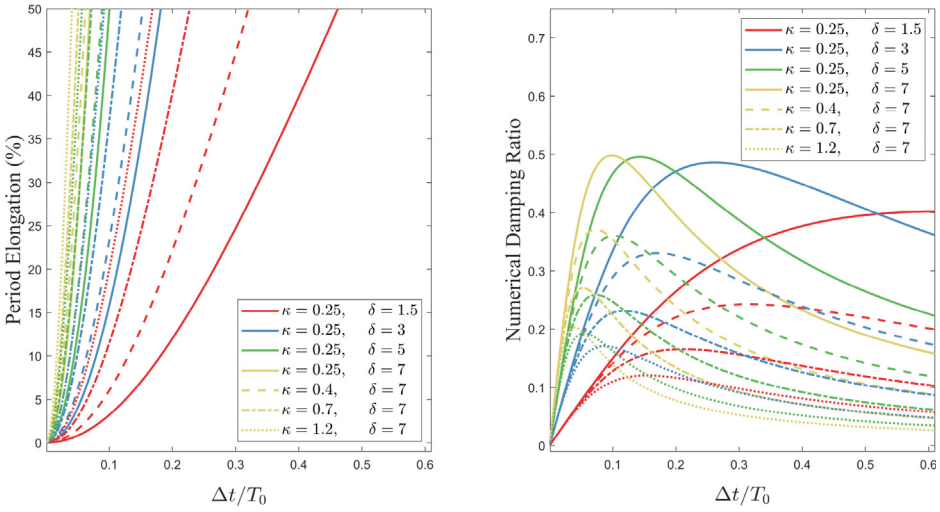

(b) Percentage period elongations and numerical damping ratio of the two-step Newmark method for $\delta \geq 1.5$

Fig. 3. The two-step Newmark method when $\xi = 0$ with $\alpha = \kappa(\delta + 0.5)^2$ for various values of κ and $\delta \geqslant 1.5$; Each color indicates a value of δ; Each line type indicates a value of κ: solid ($\kappa = 0.25$), dashed ($\kappa = 0.4$), dashed dot ($\kappa = 0.7$), dotted ($\kappa = 1.2$).

which indicates that the spectral properties of the final form of the ρ_∞-Bathe method and the two-step Newmark method can only be identical when both methods become the two-step trapezoidal rule.

In addition, we also find that, without Eqs. (7)–(9) but with $s_0 = q_0$, $s_1 = q_1$ and $s_2 = q_2$, the spectral properties of the two methods are identical when the Newmark method uses

$$\alpha = 0.25(\delta + 0.5)^2 \tag{25}$$

and the ρ_∞-Bathe method uses

$$s_0 = q_0 = \frac{-4\delta^2 + 12\delta - 1}{16\delta + 8}, \quad s_1 = q_1 = \frac{1}{2\delta + 1}, \quad s_2 = q_2 = \frac{2\delta + 1}{8}, \quad \gamma = \frac{2\delta + 1}{4} \tag{26}$$

for all δ.

With the relations in Eq. (26) and $\delta \geqslant 1/2$, the ρ_∞-Bathe method is unconditionally stable, always has complex conjugate eigenvalues, and is a first order accurate method except when $\delta = 1/2$, and then the method is the two-step trapezoidal rule. Note that with Eq. (25), the Newmark method provides the least numerical dispersion for all δ. Therefore, the two-step Newmark method is a special case of the ρ_∞-Bathe method when it provides least numerical dispersion. Hence with Eq. (26), the solid lines in Figs. 2 and 3 can be reproduced using the ρ_∞-Bathe method with the parameters in Eq. (26).

With Eq. (26), we also find a useful relation:

$$\gamma = \frac{1 - \sqrt{\rho_\infty}}{1 - \rho_\infty}; \quad \gamma_0 = 0.5 \quad \text{if } \rho_\infty = 1 \tag{27}$$

Therefore, we conclude that the relations in Eqs. (26) and (27) are the parameters to obtain a first order accurate ρ_∞-Bathe method with only one parameter, ρ_∞.

Note that the two-step Newmark method with the relations in Eq. (25) and the ρ_∞-Bathe method with the relations in Eq. (26) are identical to the β_1/β_2-Bathe method [28] with

$$\beta_1 = \frac{12\delta^2 - 4\delta + 3}{2(2\delta + 1)^2}, \quad \beta_2 = \frac{1 + 2\delta}{6 - 4\delta} \tag{28}$$

2.3. Accuracy characteristics of the ρ_∞-Bathe method and the Newmark method

The non-spurious roots of the characteristic polynomial in Eq. (20) are

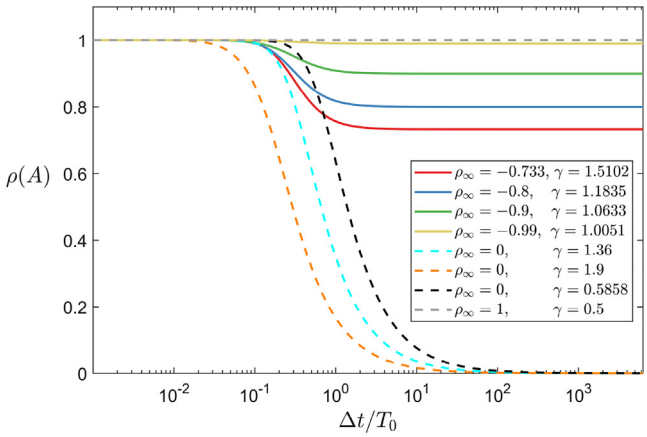

(a) Spectral radii of approximation operator of the ρ_∞- Bathe method

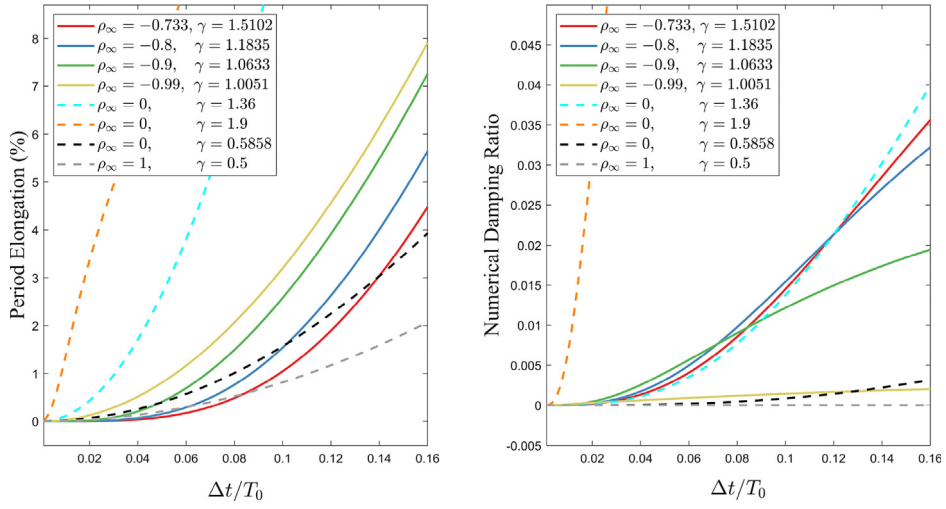

(b) Percentage period elongation and numerical damping ratio of the ρ_∞- Bathe method

Fig. 4. The ρ_∞-Bathe method when $\xi = 0$ with $\gamma = \gamma_p$ given in Eq. (38) (solid lines) and other values (dashed lines) for various values of ρ_∞.

$$\lambda_{1,2} = \left(\sqrt{A_2}, \pm\bar{\Omega}_d\right) \tag{29}$$

in polar coordinates, where

$$\bar{\Omega}_d = \begin{cases} \tan^{-1}(\sqrt{A_2 - A_1^2}/A_1) & \text{for } \Delta t \leqslant \Delta t^* \\ \tan^{-1}(-\sqrt{A_2 - A_1^2}/A_1) & \text{for } \Delta t > \Delta t^* \end{cases} \tag{30}$$

and $(A_1^2 - A_2)|_{\Delta t = \Delta t^*} = 0$ [27].

We have that the numerical damping, $\bar{\xi}$, and the period elongation, PE, are

$$\bar{\xi} = -\frac{1}{2\bar{\Omega}_0}\ln(A_2) = -\frac{1}{\bar{\Omega}_0}\ln(\rho(\mathbf{A})) \tag{31}$$

$$PE = \frac{\bar{T}_d - T_0}{T_0} = \frac{\Omega_0}{\bar{\Omega}_d} - 1 \tag{32}$$

where $\bar{T}_d$ is the "numerical natural period."

By applying the Taylor series expansion to the numerical damping, $\bar{\xi}$, we obtain, for the ρ_∞-Bathe (Eqs. (1)–(11)) and Newmark (Eqs. (12)–(17)) methods,

$$\bar{\xi}_{\rho_\infty - Bathe} = \frac{\gamma^2(\gamma-1)^2(1-\rho_\infty^2)}{8(2+\gamma(\rho_\infty - 1))^2}\Omega_0^3 + O(\Omega_0^5) \tag{33}$$

$$\bar{\xi}_{\text{Newmark}} = \frac{1}{8}(2\delta - 1)\Omega_0 + \frac{1}{128}(1-2\delta)(1-2\delta+4\alpha)\Omega_0^3 + O(\Omega_0^5) \tag{34}$$

Eqs. (33) and (34) show that the numerical damping ratio of the ρ_∞-Bathe method is $O(\Omega_0^3)$ for all values of γ and $\rho_\infty \in [0, 1)$, while the numerical damping ratio of the Newmark method is $O(\Omega_0)$ except when $\delta = 1/2$. The leading term of the numerical damping ratio of the ρ_∞-Bathe method has a local maximum at γ_0 defined in Eq. (11).

Similarly, we obtain the expressions for the period elongations of the ρ_∞-Bathe and Newmark methods as

$$PE_{\rho_\infty - Bathe} = \frac{2 - 2(\rho_\infty + 2) + 3\gamma^2(\rho_\infty + 1)}{24 + 12(\rho_\infty - 1)\gamma}\Omega_0^2 + O(\Omega_0^4) \tag{35}$$

$$PE_{Newmark} = \left(\frac{1}{8}\alpha + \frac{1}{32}\delta^2 - \frac{3}{32}\delta + \frac{11}{384}\right)\Omega_0^2 + O(\Omega_0^4) \tag{36}$$

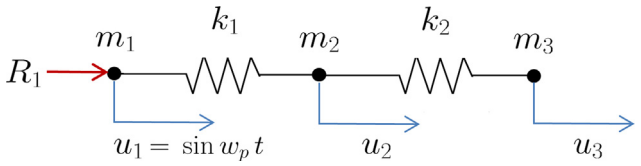

Fig. 5. Model problem of three degree-of-freedom spring system, $\omega_p = 1.2$, $m_1 = 0$, $m_2 = 1$, $m_3 = 1$, $k_1 = 10^7$, $k_2 = 1$.

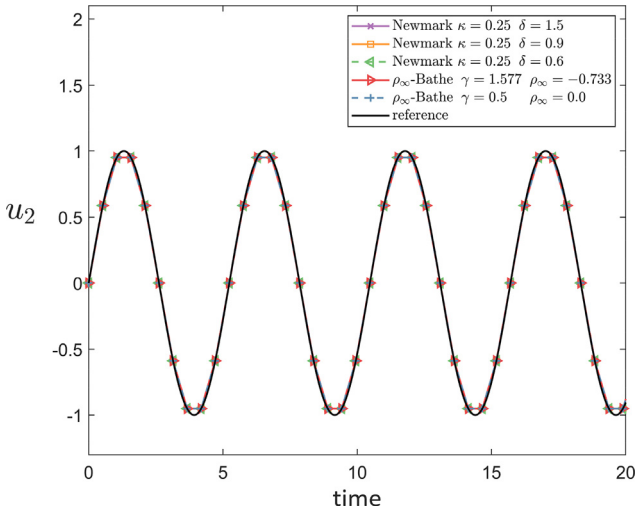

Fig. 6. Displacement of node 2 as calculated using various methods.

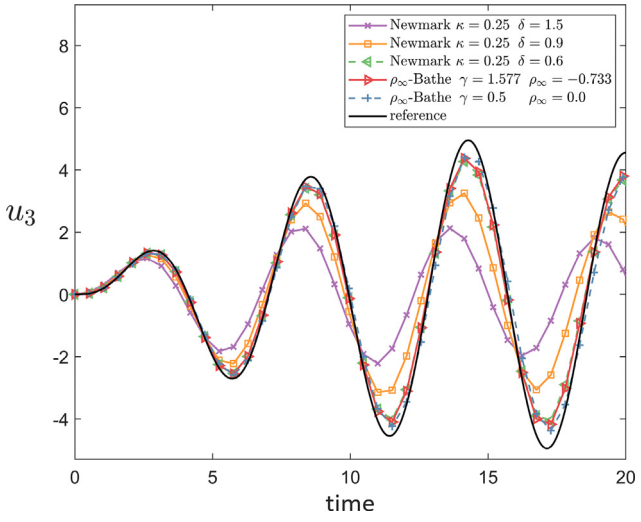

Fig. 7. Displacement of node 3 as calculated using various methods.

The period elongations of both methods are at least $O(\Omega_0^2)$. The leading term of the period elongation of the ρ_∞-Bathe method is not zero for $\rho_\infty \in [0, 1]$ and has a local minimum at γ_0 for $\rho_\infty \in [0, 1]$. For the Newmark method, the leading term is not zero and has a minimum when $\alpha = 0.25(\delta + 0.5)^2$ in the range of unconditional stability: $\delta \geqslant 0.5$ and $\alpha \geqslant 0.25(\delta + 0.5)^2$

It is also of value to consider $\rho_\infty \in [-1, 0]$. In that case, the leading term in Eq. (35) can be eliminated and the period elongation of the ρ_∞-Bathe method becomes $O(\Omega_0^4)$ when

$$\rho_\infty = \frac{3\gamma^2 - 4\gamma + 2}{\gamma(2 - 3\gamma)} \tag{37}$$

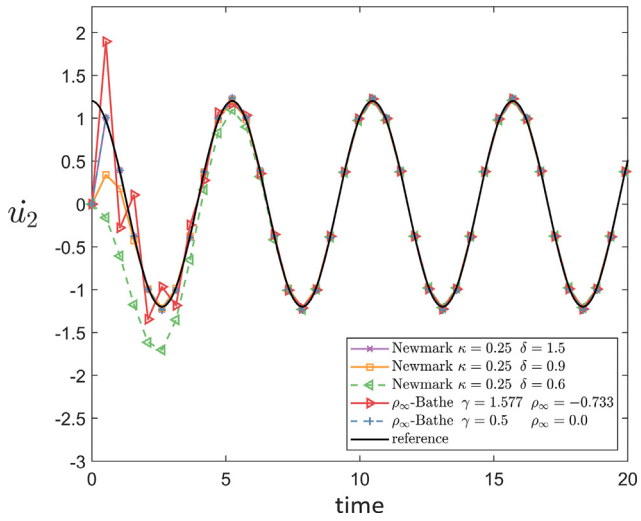

Fig. 8. Velocity of node 2 as calculated using various methods (the static correction gives the nonzero velocity at time 0.0).

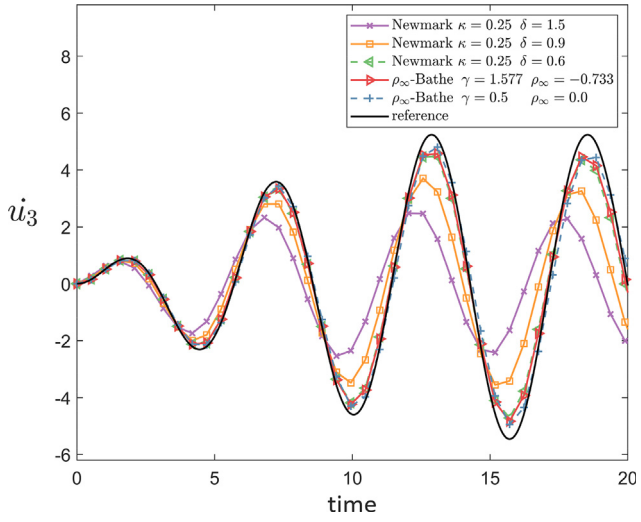

Fig. 9. Velocity of node 3 as calculated using various methods.

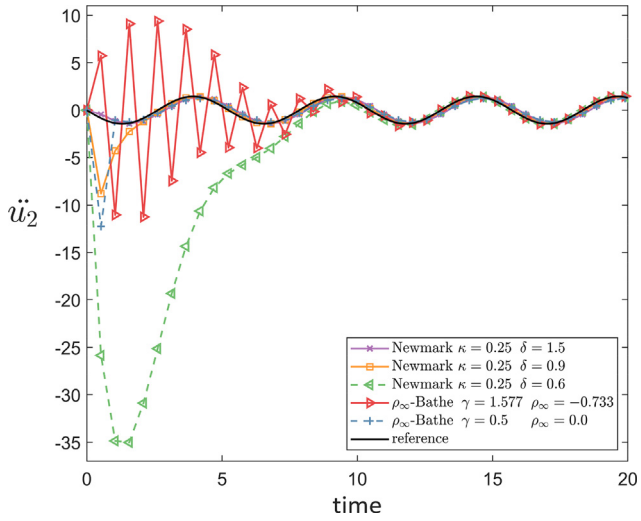

Fig. 10. Acceleration of node 2 as calculated using various methods.

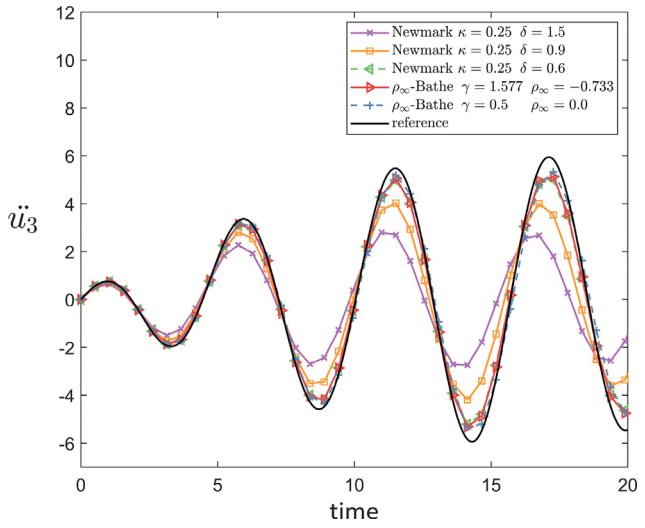

Fig. 11. Acceleration of node 3 as calculated using various methods.

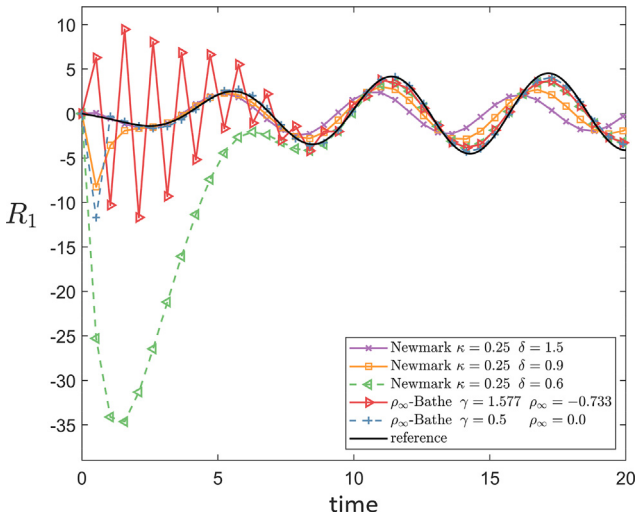

Fig. 12. Reaction force at node 1 as calculated using various methods.

Since $\gamma = 1$ is avoided in practice to not encounter a zero denominator in the constants of the method, the possible range of ρ_∞ is $\rho_\infty \in (-1, 1-\sqrt{3}]$ with $\gamma > 1$.

There are two values of γ that satisfy Eq. (37): one value with $\gamma > 1$ increases to 1.5774 and the other value decreases from ∞ to 1.5774 as ρ_∞ increases (therefore the ultimate spectral radii, $|\rho_\infty|$, decreases) from -1 to -0.7321 (values are rounded). Since both γ values provide identical spectral properties of the method, we consider the γ value in the range of $(1,\ 1.5774]$, which we call γ_p,

$$\gamma_p = \frac{\rho_\infty + 2 - \sqrt{\rho_\infty^2 - 2\rho_\infty - 2}}{3(\rho_\infty + 1)}; \quad \rho_\infty \in (-1, 1-\sqrt{3}] \tag{38}$$

Fig. 4 shows the spectral radii, period elongation and numerical damping ratio of the ρ_∞-Bathe method with γ_p for various values of $\rho_\infty \in (-1, 1-\sqrt{3}]$. We see that with γ_p, using a value for ρ_∞ close to its limit value $(1-\sqrt{3})$ provides relatively small period elongations but favourable numerical damping. However, since the negative value of ρ_∞ is limited to $\rho_\infty \in (-1, 1-\sqrt{3}]$, the spectral radius at large time steps, $\rho(\mathbf{A})|_{\Delta t=\infty}$ is also limited to $[-1+\sqrt{3},\ 1)$. Therefore, for general structural dynamics problems, $\rho_\infty = 0$ with $\gamma = 0.5$ or $2-\sqrt{2}$ is still recommended, see Section 3.1. For the solution of a problem requiring small dispersion and large numerical dissipation, but not $\rho(\mathbf{A})|_{\Delta t=\infty} = 0$, like problems of wave propagations, the negative values of ρ_∞ may be useful, see Section 3.2.

3. Illustrative numerical results

We consider a three degree-of-freedom model problem and a one-dimensional wave propagation problem to illustrate the properties of the ρ_∞-Bathe and Newmark methods. As in the above analyses and discussions we always use two equal sub-steps when employing the Newmark method for a total step of Δt.

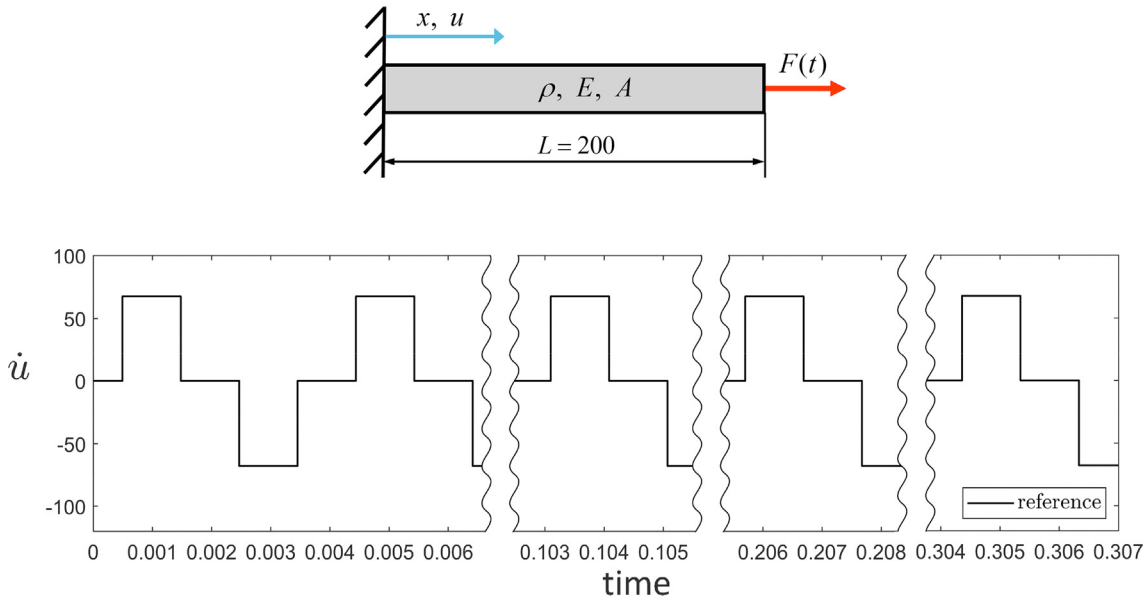

Fig. 13. A clamped bar excited by a step load, and the exact velocity at $x = 100$. Young's modulus $E = 3 \times 10^7$, mass density $\rho = 0.00073$, cross-sectional area $A = 1$, length $L = 200$.

3.1. A three degree-of-freedom model problem

The 3 degree-of-freedom model problem shown in Fig. 5 was already used in Refs. [25,27,29] to illustrate the behavior of some time integration schemes when a general structure with stiff and flexible parts is solved. We refer to Refs. [25,3] for the details of this model and comments on its importance.

Figs. 6–12 give the results obtained using the ρ_∞-Bathe and Newmark methods. For the ρ_∞-Bathe method, we consider two parameter sets: $\gamma = 0.5$ with $\rho_\infty = 0$ and $\gamma = 1.577$ with $\rho_\infty = -0.733$. For the two-step Newmark method, we use $\delta = 0.6$, 0.9 and 1.5 with $\kappa = 0.25$.

The figures show that only the ρ_∞-Bathe method with $\gamma = 0.5$ with $\rho_\infty = 0$ performs well. The ρ_∞-Bathe method with $\gamma = 1.577$ and $\rho_\infty = -0.733$ (hence $\rho(\mathbf{A})|_{\Delta t=\infty} = 0.733$) provides the least dispersion error in the low frequency range but does not give the numerical dissipation in the high frequency range important in the solution of this problem.

When using the ρ_∞-Bathe method with $\gamma = 0.5$ and $\rho_\infty = 0$, there is an overshoot in the acceleration at node 2 and in the reaction for the first time step. This overshoot can be eliminated by using a different set of α and δ only for the first sub-step, and we refer to Refs. [3,27] for details.

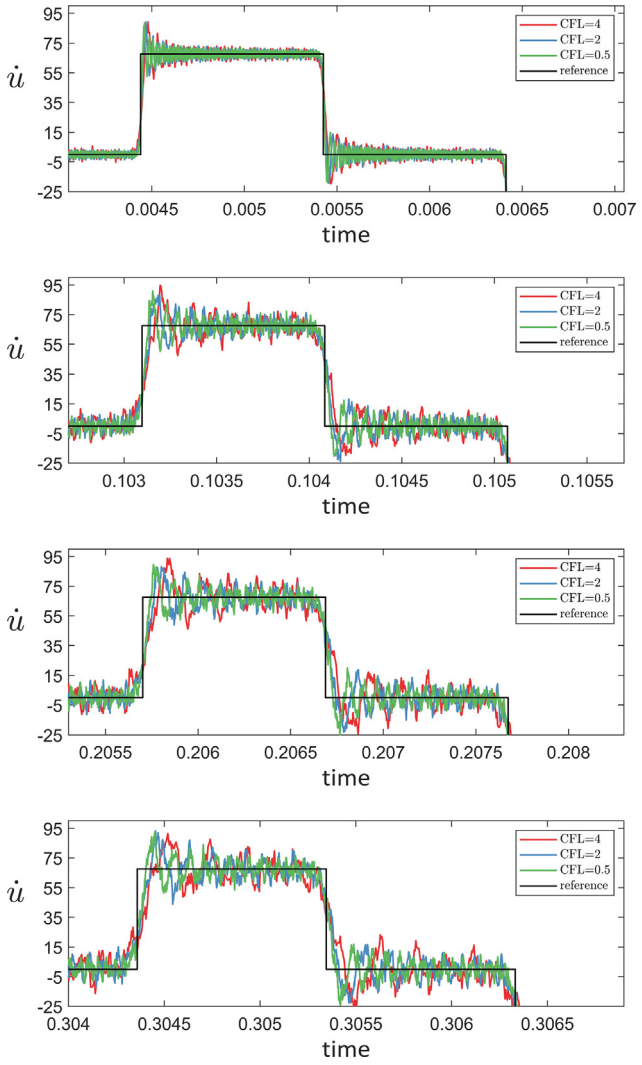

Fig. 14. Velocity at $x = 100$ predicted using the two-step Trapezoidal rule.

3.2. One-dimensional wave propagation problem

We consider a clamped bar excited by the constant step load $F(t) = 10^4$ at its end as shown in Fig. 13. We use 1000 equal size two-node elements. This problem was solved using some time integration methods in Refs. [28,29].

For the solutions, we use the trapezoidal rule, the Newmark, the β_1/β_2-Bathe and the ρ_∞-Bathe methods. We use $\gamma = 1.5774$ and $\rho_\infty = -0.7321$ for the ρ_∞-Bathe method, $\delta = 0.6$ and 1.5 with $\kappa = 0.25$ for the Newmark method, and $\beta_1 = 0.39$ and $\beta_2 = 2\beta_1$ for the β_1/β_2-Bathe method. Note that all the considered methods are special cases of the ρ_∞-Bathe method, see Section 2.2 and Ref. [29].

The time step sizes used are determined by the CFL number, which is the ratio of the propagation length per time step (using the exact wave speed) to the element size: $\Delta t = \text{CFL} \times 9.8658 \times 10^{-7}$. We consider various CFL numbers for each method.

Figs. 14–18 show the velocity at the center of the bar (at node 500) calculated using the methods with various CFL numbers, at three different time windows. For the first time window (t = 0.004–0.007) the methods considered (except for the trapezoidal rule) provide good results. In particular, the first-order accurate methods, the Newmark method with $\delta = 0.6$ and $\kappa = 0.25$ and

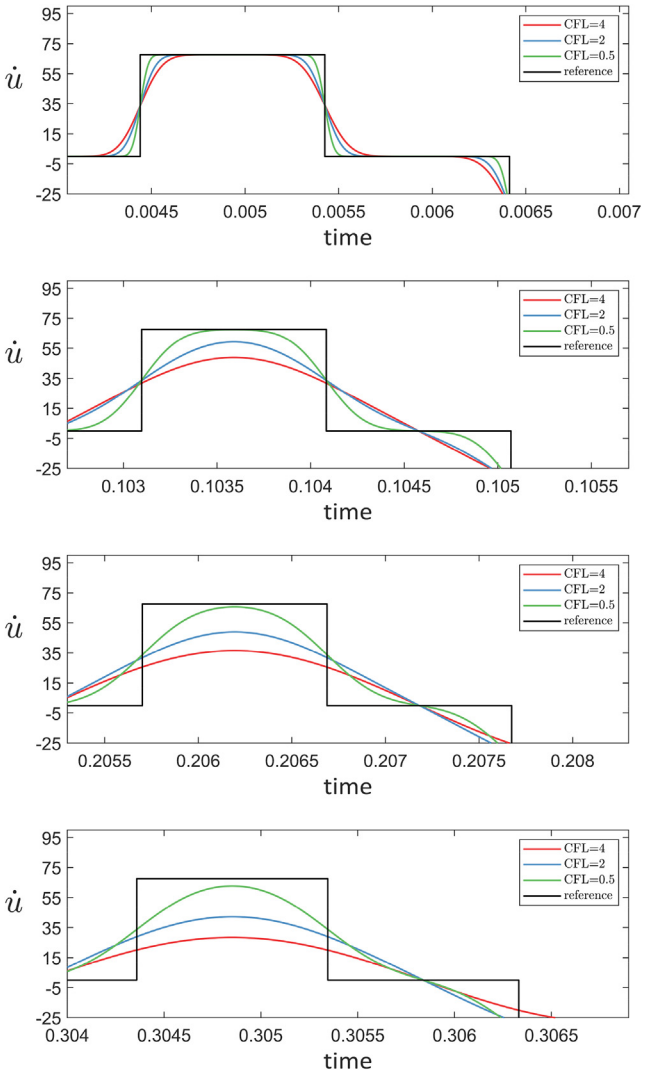

Fig. 15. Velocity at $x = 100$ predicted using the two-step Newmark method ($\kappa = 0.25$, $\delta = 1.5$).

the β_1/β_2-Bathe method with $\beta_1 = 0.39$ and $\beta_2 = 2\beta_1$, provide very accurate solutions for this time window. The results using the trapezoidal rule show significant spurious oscillations.

As time increases, however, the solution accuracy using the first-order accurate methods deteriorates due to large numerical damping in the low frequency range (see, Fig. 3(b)) while the results using the ρ_∞-Bathe method remain quite accurate (Fig. 18). Using the ρ_∞-Bathe method, with $\gamma = 1.5774$, $\rho_\infty = -0.7321$ the solution accuracy only deteriorates mildly with time due to the small numerical damping in the low frequencies, see Fig. 4(b).

Among the CFL numbers considered, using the smaller CFL number provided in this example more accurate solutions when using the Newmark and Bathe methods as first-order accurate schemes. However, a further study is needed to identify the CFL numbers for optimal accuracy of the methods considering the various values of parameters [40–42].

4. Concluding remarks

We considered in this paper the Newmark and Bathe time integration schemes for the solution of structural dynamics and wave propagation problems. The Newmark scheme and in particular the trapezoidal rule are widely used in engineering and scientific studies.

We first focused on the unconditionally stable Newmark method with $\delta \geqslant 0.5$ and $\alpha = \kappa(\delta + 0.5)^2$, $\kappa = 0.25$ and showed that the Newmark method (using two equal sub-steps per time step) is then a special case of the Bathe method, and that with these parameters the Newmark method provides the maximum numerical dissipation and minimum numerical dispersion for a given δ. As widely known when $\delta = 0.5$ the second-order accurate trapezoidal rule is obtained, otherwise the Newmark method is first-order accurate. The trapezoidal rule is obtained in the ρ_∞-Bathe method with $\rho_\infty = 1.0$ and two equal sub-steps ($\gamma = 0.5$). Of course, when the parameters in the ρ_∞-Bathe method are selected to correspond to the Newmark method, the same solution accuracy is achieved. We also showed that the β_1/β_2-Bathe method [28] can be obtained by choosing the appropriate parameters in the ρ_∞-Bathe scheme, see also Ref. [29].

We found that by varying κ and δ in the Newmark method and considering the numerical dissipation, only the values $\kappa = 0.25$ and $0.5 \leqslant \delta \leqslant 1.5$ are of interest, because for other values the numerical dissipation does not increase monotonically as the time step value increases.

The usual ρ_∞-Bathe method uses two parameters, $\rho_\infty = [0, 1]$ and γ, but the optimal value of γ for maximum amplitude decay

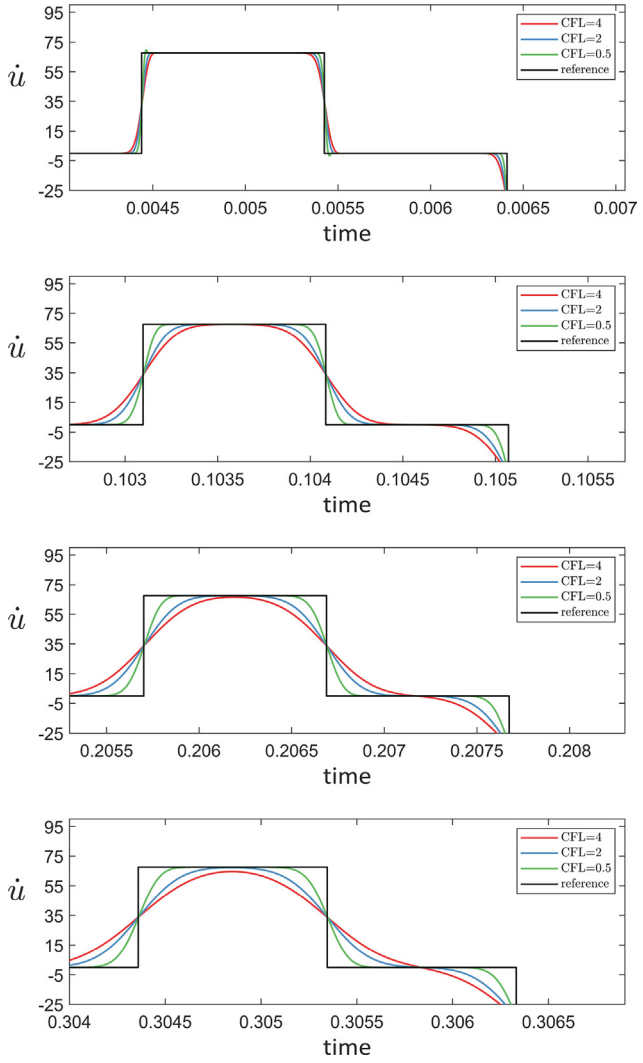

Fig. 16. Velocity at $x = 100$ predicted using the two-step Newmark method ($\kappa = 0.25$, $\delta = 0.6$).

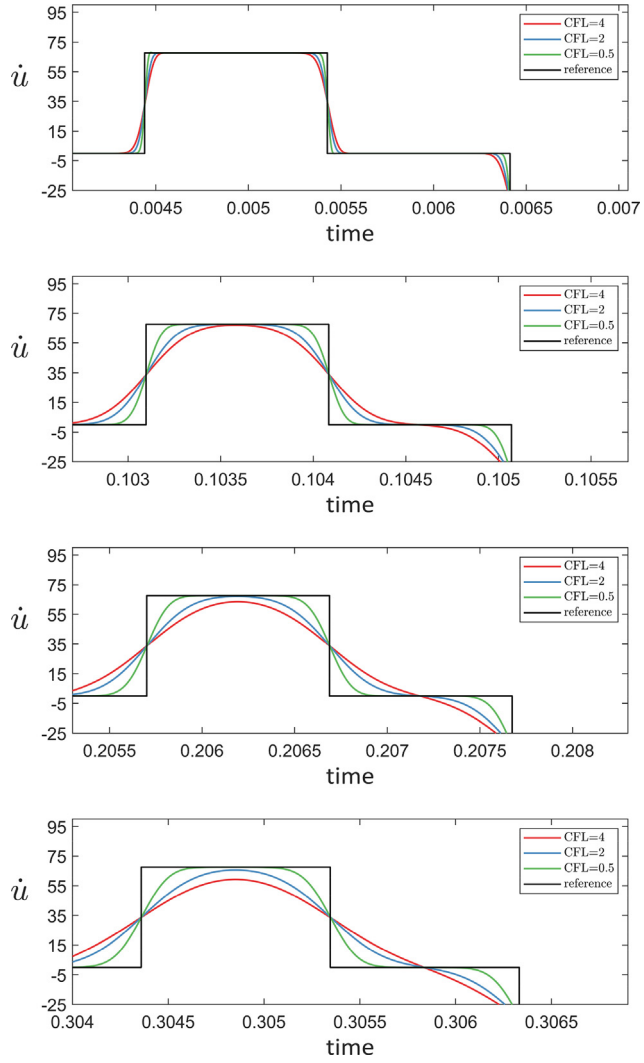

Fig. 17. Velocity at $x = 100$ predicted using the β_1/β_2-Bathe method ($\beta_1 = 0.39$, $\beta_2 = 2\beta_1$).

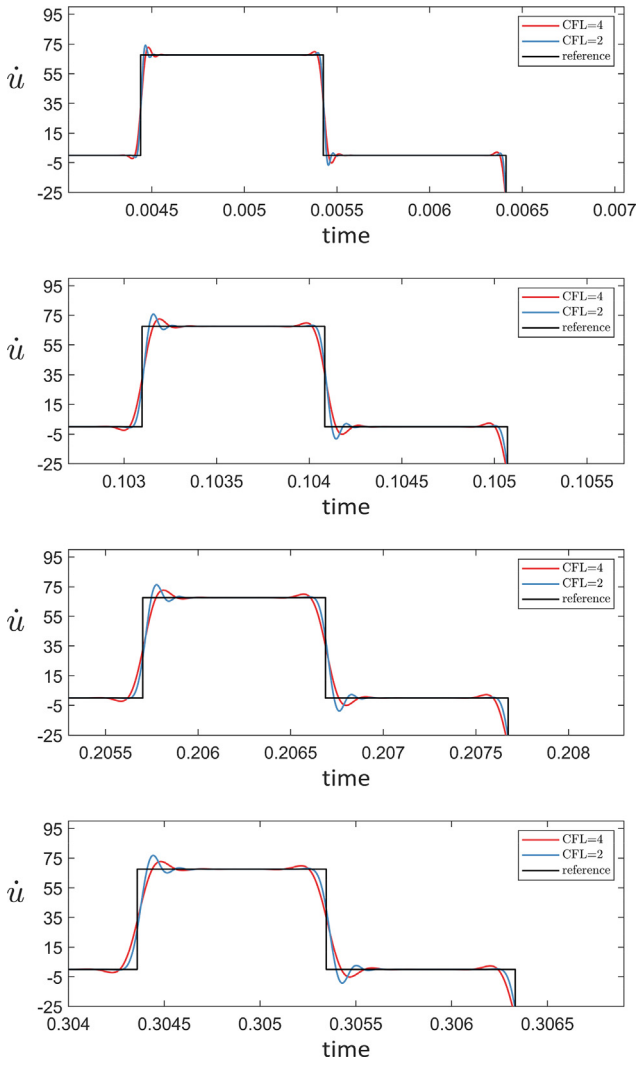

Fig. 18. Velocity at $x = 100$ predicted using the ρ_∞-Bathe method ($\gamma = 1.5774$, $\rho_\infty = -0.7321$).

and minimum period elongation is given as a function of ρ_∞, hence we have a one-parameter time integration scheme. With the optimal value of γ, the amplitude decay and period elongation are almost the same as when using $\gamma = 0.5$.

While the curves of numerical dissipation in the ρ_∞-Bathe method show very little dissipation at small time step values that rapidly increases as the time step becomes larger, which is very valuable, the curves for the Newmark method for any κ and δ considered here do not have this desirable curvature.

We also considered the values $\gamma > 1$ and $\rho_\infty = [-1, 0]$ and found that for some analyses, values other than $\rho_\infty = [0, 1]$ and the corresponding optimal value of γ can be effective parameters to use.

We illustrated the findings of our theoretical study in example solutions. These solutions exemplify that the ρ_∞-Bathe method with $\rho_\infty = 0.0$ and $\gamma = 0.5$ (or $\gamma = \gamma_0$ for less computations in linear analysis) is most effective in structural dynamics when stiff and flexible parts are considered. Further, in the solution of a one-dimensional wave propagation problem, we found that the ρ_∞-Bathe method is more effective than the Newmark method. The trapezoidal rule shows significant oscillations at the wave fronts, and when the Newmark method is employed with $\delta > 0.5$, the solution is quite accurate for small solution times but not for larger times because the method is then only first-order accurate. The same observations hold when using the β_1/β_2-Bathe method.

On the other hand, when we used the ρ_∞-Bathe method, with $\rho_\infty < 0$ and $\gamma > 1.5$ good results have been obtained for short and longer times in the wave propagation problem. We employed here $\rho_\infty \approx -0.75$ and $\gamma \approx 1.6$; however, further studies are needed to establish the optimal parameters in the ρ_∞-Bathe scheme for the solution of wave propagation problems [42].

Acknowledgment

This work was partly supported by the Ministry of Trade Industry & Energy (MOTIE, Korea), Ministry of Science & ICT (MSIT, Korea), and Ministry of Health & Welfare (MOHW, Korea) under Technology Development Program for AI-Bio-Robot-Medicine Convergence (20001655).

Appendix A. The two-step Newmark method with $\alpha = 1/4$, $\delta = 1/2$ and the ρ_∞-Bathe method with $\rho_\infty = 1$ and $\gamma = 1/2$ are identical

When $\alpha = 1/4$, $\delta = 1/2$, $\rho_\infty = 1$ and $\gamma = 1/2$, it is clear that the relations in the first sub-steps of the two-step Newmark method and the ρ_∞-Bathe method are identical as

$$ {}^{t+\Delta t/2}\dot{\mathbf{U}} = {}^{t}\dot{\mathbf{U}} + [{}^{t}\ddot{\mathbf{U}} + {}^{t+\Delta t/2}\ddot{\mathbf{U}}](\Delta t/4) \tag{A1} $$

$$ {}^{t+\Delta t/2}\mathbf{U} = {}^{t}\mathbf{U} + {}^{t}\dot{\mathbf{U}}(\Delta t/2) + [{}^{t}\ddot{\mathbf{U}} + {}^{t+\Delta t/2}\ddot{\mathbf{U}}](\Delta t^2/16) \tag{A2} $$

In the second sub-step, the two-step Newmark method, with $\alpha = 1/4$, $\delta = 1/2$, Eqs. (16) and (17) becomes

$$ {}^{t+\Delta t}\dot{\mathbf{U}} = {}^{t+\Delta t/2}\dot{\mathbf{U}} + [{}^{t+\Delta t/2}\ddot{\mathbf{U}} + {}^{t+\Delta t}\ddot{\mathbf{U}}](\Delta t/4) \tag{A3} $$

$$ {}^{t+\Delta t}\mathbf{U} = {}^{t+\Delta t/2}\mathbf{U} + {}^{t+\Delta t/2}\dot{\mathbf{U}}(\Delta t/2) + [{}^{t+\Delta t/2}\ddot{\mathbf{U}} + {}^{t+\Delta t}\ddot{\mathbf{U}}](\Delta t^2/16) \tag{A4} $$

With Eqs. (A1) and (A2), Eqs. (A3) and (A4) can be rewritten as

$$ {}^{t+\Delta t}\dot{\mathbf{U}} = {}^{t}\dot{\mathbf{U}} + [{}^{t}\ddot{\mathbf{U}} + 2^{t+\Delta t/2}\ddot{\mathbf{U}} + {}^{t+\Delta t}\ddot{\mathbf{U}}](\Delta t/4) \tag{A5} $$

$$ {}^{t+\Delta t}\mathbf{U} = {}^{t}\mathbf{U} + {}^{t}\dot{\mathbf{U}}\Delta t + [3^{t}\ddot{\mathbf{U}} + 4^{t+\Delta t/2}\ddot{\mathbf{U}} + {}^{t+\Delta t}\ddot{\mathbf{U}}](\Delta t^2/16) \tag{A6} $$

In the ρ_∞-Bathe method with $\rho_\infty = 1$ and $\gamma = 1/2$, the parameters become $s_0 = q_0 = s_2 = q_2 = 1/4$ and $s_1 = q_1 = 1/2$. Thus, the relations in the second sub-step, Eqs. (5) and (6), become

$$ {}^{t+\Delta t}\mathbf{U} = {}^{t}\mathbf{U} + ({}^{t}\dot{\mathbf{U}} + 2^{t+\Delta t/2}\dot{\mathbf{U}} + {}^{t+\Delta t}\dot{\mathbf{U}})(\Delta t/4) \tag{A7} $$

$$ {}^{t+\Delta t}\dot{\mathbf{U}} = {}^{t}\dot{\mathbf{U}} + ({}^{t}\ddot{\mathbf{U}} + 2^{t+\Delta t/2}\ddot{\mathbf{U}} + {}^{t+\Delta t}\ddot{\mathbf{U}})(\Delta t/4) \tag{A8} $$

With Eqs. (A1) and (A2), Eqs. (A7) and (A8) can be rewritten as

$$ {}^{t+\Delta t}\dot{\mathbf{U}} = {}^{t}\dot{\mathbf{U}} + [{}^{t}\ddot{\mathbf{U}} + 2^{t+\Delta t/2}\ddot{\mathbf{U}} + {}^{t+\Delta t}\ddot{\mathbf{U}}](\Delta t/4) \tag{A9} $$

$$ {}^{t+\Delta t}\mathbf{U} = {}^{t}\mathbf{U} + {}^{t}\dot{\mathbf{U}}\Delta t + [3^{t}\ddot{\mathbf{U}} + 4^{t+\Delta t/2}\ddot{\mathbf{U}} + {}^{t+\Delta t}\ddot{\mathbf{U}}](\Delta t^2/16) \tag{A10} $$

which are the relations in the second sub-step of the two-step Newmark method, Eqs. (A5) and (A6).

References

[1] Bathe KJ. The finite element method. In: Linderberg T, Wah B, editors. Encyclopedia of computer science and engineering. Hoboken (New Jersey): J. Wiley and Sons; 2009. p. 1253–64.
[2] Bathe KJ. Frontiers in finite element procedures & applications. In: Topping BHV, Iványi P, editors. Chapter 1 in Computational methods for engineering technology. Stirlingshire (Scotland): Saxe-Coburg Publications; 2014.
[3] Bathe KJ. Finite element procedures. 2nd ed. Watertown (MA): K.J. Bathe; 2016 [also published by Higher Education Press China] http://meche.mit.edu/people/faculty/kjb@mit.edu.
[4] Houbolt JC. A recurrence matrix solution for the dynamic response of aircraft. J Aeronaut Sci 1950;17:540–50.

[5] Newmark NM. A method of computation for structural dynamics. J Eng Mech Div (ASCE) 1959;85:67–94.
[6] Collatz L. The numerical treatment of differential equations. 3rd ed. Springer-Verlag; 1966.
[7] Wilson EL. A computer program for the dynamic stress analysis of underground structures SEL report. University of California at Berkeley; 1968. p. 68–71.
[8] Wilson EL, Farhoomand I, Bathe KJ. Nonlinear dynamic analysis of complex structures. Int J Earthquake Eng Struct Dyn 1973;1:241–52.
[9] Bathe KJ, Wilson EL. Stability and accuracy analysis of direct integration methods. Int J Earthquake Eng Struct Dyn 1973;1:283–91.
[10] Hilber HM, Hughes TJR, Taylor RL. Improved numerical dissipation for time integration algorithms in structural dynamics. Earthquake Eng Struct Dyn 1977;5:283–92.
[11] Wood WL, Bossak M, Zienkiewicz OC. An alpha modification of Newmark's method. Int J Numer Meth Eng 1980;15:1562–6.
[12] Shao HP, Cai CW. The direct integration three-parameters optimal schemes for structural dynamics. In: Proceedings of the international conference: machine dynamics and engineering applications. Xi'an Jiaotong University Press; 1988. p. C16–20.
[13] Dokainish MA, Subbaraj K. A survey of direct time-integration methods in computational structural dynamics—I. Explicit methods. Comput Struct 1989;32:1371–86.
[14] Subbaraj K, Dokainish MA. A survey of direct time-integration methods in computational structural dynamics—II. Implicit methods. Comput Struct 1989;32:1387–401.
[15] Chung J, Hulbert GM. A time integration algorithm for structural dynamics with improved numerical dissipation: the generalized-alpha method. J Appl Mech (ASME) 1993;60:371–5.
[16] Tamma KK, Zhou X, Sha D. The time dimension: a theory towards the evolution, classification, characterization and design of computational algorithms for transient/dynamic applications. Arch Comput Methods Eng 2000;7:67–290.
[17] Tamma KK, Sha D, Zhou X. Time discretized operators. Part 1: Towards the theoretical design of a new generation of a generalized family of unconditionally stable implicit and explicit representations of arbitrary order for computational dynamics. Comput Methods Appl Mech Eng 2003;192:257–90.
[18] Sha D, Zhou X, Tamma KK. Time discretized operators. Part 2: Towards the theoretical design of a new generation of a generalized family of unconditionally stable implicit and explicit representations of arbitrary order for computational dynamics. Comput Methods Appl Mech Eng 2003;192:291–329.
[19] Zhou X, Tamma KK. Design, analysis, and synthesis of generalized single step single solve and optimal algorithms for structural dynamics. Int J Numer Meth Eng 2004;59:597–668.
[20] Chang SY. A family of noniterative integration methods with desired numerical dissipation. Int J Numer Meth Eng 2014;100(1):62–86.
[21] Chang SY. Dissipative, noniterative integration algorithms with unconditional stability for mildly nonlinear structural dynamic problems. Nonlinear Dyn 2015;79(2):1625–49.
[22] Malakiyeh MM, Shojaee S, Javaran SH. Development of a direct time integration method based on Bezier curve and 5th-order Bernstein basis function. Comput Struct 2018;194:15–31.
[23] Bathe KJ, Baig MMI. On a composite implicit time integration procedure for nonlinear dynamics. Comput Struct 2005;83:2513–24.
[24] Bathe KJ. Conserving energy and momentum in nonlinear dynamics: a simple implicit time integration scheme. Comput Struct 2007;85:437–45.
[25] Bathe KJ, Noh G. Insight into an implicit time integration scheme for structural dynamics. Comput Struct 2012;98–99:1–6.
[26] Zhang J, Liu Y, Liu D. Accuracy of a composite implicit time integration scheme for structural dynamics. Int J Numer Meth Eng 2017;109:368–406.
[27] Noh G, Bathe KJ. Further insights into an implicit time integration scheme for structural dynamics. Comput Struct 2018;202:15–24.
[28] Malakiyeh MM, Shojaee S, Bathe KJ. The Bathe time integration method revisited for prescribing desired numerical dissipation. Comput Struct 2019;212:289–98.
[29] Noh G, Bathe KJ. The Bathe time integration method with controllable spectral radius: the ρ_∞-Bathe method. Comput Struct 2019;212:299–310.
[30] Dong S. BDF-like methods for nonlinear dynamic analysis. J Comput Phys 2010;229(8):3019–45.
[31] Noh G, Bathe KJ. An explicit time integration scheme for the analysis of wave propagations. Comput Struct 2013;129:178–93.
[32] Soares D. A novel family of explicit time marching techniques for structural dynamics and wave propagation models. Comput Methods Appl Mech Eng 2016;311:838–55.
[33] Wen WB, Wei K, Lei HS, Duan SY, Fang DN. A novel sub-step composite implicit time integration scheme for structural dynamics. Comput Struct 2017;182:176–86.
[34] Wen W, Tao Y, Duan S, Yan J, Wei K, Fang D. A comparative study of three composite implicit schemes on structural dynamic and wave propagation analysis. Comput Struct 2017;190:126–49.
[35] Kwon S-B, Lee J-M. A non-oscillatory time integration method for numerical simulation of stress wave propagations. Comput Struct 2017;192:248–68.
[36] Kim W, Choi SY. An improved implicit time integration algorithm: the generalized composite time integration algorithm. Comput Struct 2018;196:341–54.
[37] Zhang HM, Xing YF. Optimization of a class of composite method for structural dynamics. Comput Struct 2018;202:60–73.
[38] Kim W, Lee JH. An improved explicit time integration method for linear and nonlinear structural dynamics. Comput Struct 2018;206:42–53.
[39] Li J, Yu K. An alternative to the Bathe algorithm. Appl Math Model 2019;69:255–72.
[40] Noh G, Ham S, Bathe KJ. Performance of an implicit time integration scheme in the analysis of wave propagations. Comput Struct 2013;123:93–105.
[41] Kim KT, Zhang L, Bathe KJ. Transient implicit wave propagation dynamics with overlapping finite elements. Comput Struct 2018;199:18–33.
[42] Kwon S-B, Bathe KJ, Noh G. Performance of Bathe time integration schemes in the analysis of wave propagations [in preparation].